http://dx.doi.org/10.14500/aro.12222

Modification of the Optical Properties of Polyvinyl Alcohol through Incorporating Cu_2O Nanoparticles Prepared by Laser Ablation

Chro H. Othman, Mohammed F. M. Sabri† and Simko O. Ramadan

Department of Physics, Faculty of Science and Health, Koya University,
Danielle Mitterrand Boulevard, Koya KOY45, Kurdistan Region – F.R. Iraq

***Abstract*—A focused, high-intensity pulsed laser ablated 99.9% - pure copper targets submerged in deionized water and in Polyvinyl alcohol (PVA) solution, respectively, was utilized to produce Cu_2O nanoparticles (NPs). Nano-plasmonic cuprous oxide was incorporated using the nanosecond Nd: YAG pulsed laser ablation in liquids technique, which advances the physiochemical characteristics of Cu_2O/PVA nanocomposite. Optical characterization was carried out for the induced Cu_2O NPs and Cu_2O/PVA nanocomposites with six different mass concentrations of Cu_2O. The concentrations of the Cu_2O NPs were 0.007, 0.017, 0.027, 0.04, 0.047, and 0.057 mg/mL in the PVA matrix. X-ray diffraction confirms that copper ions were reduced to form crystalline Cu_2O NPs. Furthermore, DLS showed the presence of NP agglomeration, which revealed polydispersity of Cu_2O NPs. The band gap of pristine PVA, determined from Tauc plots, was 5.00 eV. The optical band gap decreased progressively with increasing mass concentration of Cu_2O NPs. This band-gap reduction is attributed to changes in the PVA electronic structure caused by incorporated Cu_2O NPs. A distinctive feature of this work is the use of pulsed-laser ablation in liquid to generate plasmonic Cu_2O NPs and incorporate them *in situ* into PVA at room temperature in a single step; NP concentration was precisely controlled by the number of laser pulses.**

***Index Terms*—Cu_2O NPs, PVA, Nanocomposite, Nd: YAG laser, Laser ablation.**

I. Introduction

At present, thin-film solar cells based on Cu_2O absorbers are considered promising alternatives to state-of-the-art silicon solar cells (Naz, et al., 2023). The thermal reduction of copper oxide to metal may be accomplished at elevated temperatures, and solar cells utilizing these absorbers will be economically viable due to their direct bandgap, high absorption coefficient, and the plentiful availability of copper in the Earth's crust (Oluyemi, et al., 2023). Copper oxide nanoparticles (NPs) are prevalent in nature and are cost-effective materials. They exhibit fascinating physicochemical properties and exist in multiple oxidation states, specifically CuO and Cu_2O. They possess an approximate band gap energy of 2 eV and have garnered considerable importance due to their chemical inertness and thermal stability. In addition, Cu_2O NPs are inorganic and far more stable than organic NPs and are of p-type semiconductors characterized by monoclinic nanostructures. The controllability of synthetic processes is essential for generating NPs with a particular size and form (Madkhali, 2024). Cu_2O is of a group I-IV compound semiconductor in the periodic table, notable for its high optical absorption, high electrical conductivity, non-toxicity, and cost-effective fabrication (Li, et al., 2025), as well as a wide range of applications in gas sensors (Kumar, et al., 2023). This causes a measurable change in electrical resistance when the material is exposed to gas (Maier, et al., 2025, Mushtaq, et al., 2022). It is a significant semiconductor material related to its dual stability in two semiconducting phases. Specifically, cuprous oxide (Cu_2O) and cupric oxide (CuO). The oxides exhibit significant differences in physical characteristics, electrical conductivities, colors, and crystalline structures (Kaur, et al., 2022).

A wide variety of methods have been developed to synthesis Cu_2O in various forms to date. Chemical vapor deposition, electrodeposition, sputtering, and sol-gel dip coating are among these ways; but pulsed laser ablation (PLA) is the most effective and affordable technique currently available (Aziz, Nayef and Rasheed, 2025) to synthesis pure, uncontaminated nanostructures and a necessity for their eventual usage in electronics or energy. PLA is an easy, fast, and straightforward method for NPs generation as compared to other methods. It does not require long reaction times, high temperatures, or multi-step chemical synthetic procedures. It does not require the use of toxic, adverse, or pyrophoric chemical precursors for nanomaterial creation, providing it beneficial to the environment (Zhan, et al., 2024). Formation of NPs by means of laser ablation in liquids (LAL) have recently been employed in a variety of novel applications, such as friction reduction, the development of solar

ARO-The Scientific Journal of Koya University
Vol. XIII, No.2 (2025), Article ID: ARO.12222. 12 pages
DOI: 10.14500/aro.12222
Received: 19 April 2025; Accepted: 28 October 2025
Regular research paper; Published: 02 December 2025
†Corresponding author's e-mail: mohammed.mohammedsabri@koyauniversity.org

nanofluids, and optical limiting devices. The synthesis of NPs using LALs encounters obstacles, such as achieving exact dimensions and morphologies, minimizing polydispersity, and improving productivity.

When laser pulses are directed at a medium containing Cu_2O NPs, the energy from the laser can induce numerous physical and chemical transformations. The alterations are contingent upon the laser's strength, duration, and wavelength. More intense laser pulses can induce localized heating, leading to the evaporation or melting of some components, hence affecting the concentration of Cu_2O NPs. This is especially applicable if the laser intensity is suitable to induce ablation or melting of the material. As the laser pulse frequency was raised, the energy deposited on the copper target improved the ablation process, causing an increased ejection of copper material in the medium, and this resulted in an increase in the concentration of Cu_2O NPs. The promise of low-cost processing techniques and favorable electrochemical properties makes Cu_2O one of the leading materials for electrical, optical, and sensor applications. NPs formed by PLA require a liquid medium for stabilization and dispersion. The tiny particles that aggregate in the liquid are referred to as cuprous oxide NPs (Cu_2O NPs) and consist of copper oxide. The ultimate size and morphology of such particles are affected by variables, such as laser intensity, pulse duration, wavelength, ablation duration, and the types of metal and liquid involved (Kudhur, et al., 2024). The produced NPs require a stabilizing component to avoid agglomeration (Szczyglewska, Feliczak-Guzik and Nowak, 2023).

Polyvinyl alcohol (PVA) is identified to be a proximate host matrix for Cu_2O NPs due to its high tensile strength, thermal stability, hydrophilic properties, and minimal clustering. Recently, different types of all nanofillers are used to improve the properties of PVA. PVA carbon chain also contains a few hydroxyl groups, which render them as hydrogen bond donors with the Cu_2O nanofiller; a crucial step in producing nanocomposites. Due to the optical properties of PVA, which have been customized for nanofillers, it is a promising candidate for optical electronics applications. Optical absorption and band gap are essential in optoelectronic devices. Controlling the band gap is one of the critical processes in converting novel materials for optoelectronic devices (Kimar and Al-Nesrawy, 2024, Alruwaili, et al., 2025). The large optical band gap of the PVA matrix precludes the absorption of near-infrared radiation. Consequently, diminished light can be perceived. Consequently, pure PVA is the sole partial polymer utilized in the active layer of organic solar cells. Substituting this polymer with one possessing a reduced band gap can resolve the aforementioned issue. This task can be accomplished by incorporating nano-inorganic components into the polymeric backbone (Seimela, 2022). PVA is useful in capacitors and high-voltage AC/DC cables (Malik, et al., 2022).

Experimental validation of the electrical structure of copper oxide phases has notably given scant study attention (Oluyemi, et al., 2023). The concentration of cuprous oxide (Cu_2O) in PVA-based nanocomposites improves their electrical, mechanical, and optical properties. The stable oxide phases, Cu_2O and CuO, are important in semiconductor applications because of their distinct characteristics. A uniform distribution of Cu_2O within PVA increases the dielectric constant and AC conductivity, thereby improving the material's performance for technological applications. Consistent dispersion is essential for preventing agglomeration and achieving uniform properties (Al-Hakimi, et al., 2023). So that, in a Cu_2O/PVA nanocomposite, PVA plays several crucial roles as the host matrix, such as: First, stabilization and dispersion; the abundant – OH groups along the PVA backbone form hydrogen bonds with nascent Cu_2O nuclei, effectively "capping" growing particles and preventing their uncontrolled aggregation. This chemical reaction produces a uniform dispersion of Cu_2O NPs throughout the film or hydrogel (Zhang, et al., 2023). Second, controlled nucleation and growth; during *in situ* NP formation, the polymer chains of PVA act as a soft template that regulates local supersaturation. This templating effect yields Cu_2O crystallites of narrow, tunable size and morphology (Zhang, et al., 2023, Kimar and Al-Nesrawy, 2024). Third, optical transparency and processability; Due to its excellent water solubility and film-forming capability, PVA produces smooth, crack-free, visibly transparent coatings that allow optical access to the embedded Cu_2O for plasmonic or photocatalytic applications (Kimar and Al-Nesrawy, 2024). Fourth, barrier protection and environmental stability; PVA encapsulation slows down oxidation ($Cu_2O \rightarrow CuO$) and shields NPs from agglomeration or leaching (Zhang, et al., 2023).

Researchers recently examined the effects of incorporating small amounts (0.1–0.5 wt%) of nano- Cu_2O fillers into PVA composite films. Well-dispersed fillers that adhered to internal surfaces improved mechanical properties, including tensile strength and Young's modulus. Significant changes in optical properties were observed: the direct band gap decreased from 5.29 eV to 3.16 eV, indicating potential applicability in optoelectronic devices (Griffin, et al., 2022, Kanchana, Vanitha and Basavaraj, 2023a). Over the past decades, Cu_2O thin films have been extensively applied in various technological areas to explore their possible applications in solar cell fabrication, semiconductor sensors, electrochemical devices, and photovoltaic materials (Awal, et al., 2024, Abdelfatah, et al., 2023). Nanostructured Cu_2O is combined with natural colors, such as chlorophyll to make solar cells more efficient by making more electrons available (Awal, et al., 2024, Abdulnabi and Juda, 2023).

Copper oxide NPs demonstrated enhanced performance as nanofluids in thermal transfer applications. It can also be used to get rid of dyes, power photovoltaic systems, clean wastewater, make batteries, grow crops, make textiles, and keep food fresh. Hence, it is important to make copper oxide NPs with precise, programmable sizes, shapes, and structures. *Spondias mombin* peel extract works well for making Pd NPs (Oluyemi, et al., 2023). In composite propellants, copper oxide is also used as a combustion catalyst. (Mirzajani, et al., 2022). Nanostructured Cu_2O is frequently employed in thin-film solar cells as an absorber layer. The combustion of fossil fuels for electricity generation has adversely affected the environment; thus, the adoption of renewable energy sources

http://dx.doi.org/10.14500/aro.12222

as an alternative to fossil fuels has become imperative (Zhang, et al., 2023, Oluyemi, et al., 2023). A novel aspect of this work is the use of PLA in liquid (PLAL) to generate plasmonic Cu_2O NPs and embed them *in situ* into a PVA matrix through a single-step, room-temperature process. By varying the number of laser pulses, the NP concentration can be precisely controlled, yielding tunable optical properties, such as a plasmonic bandgap that are beneficial for photocatalysis and solar-energy applications. To our knowledge, synthesizing Cu_2O/PVA nanocomposites by PLAL with variable pulse counts has not been reported before. The primary objective of this study is therefore to systematically investigate how changing the laser pulse count influences the optical properties of the resulting Cu_2O/PVA nanocomposites.

II. Experimental Procedures

A. Materials

High-purity copper target (99.99%), PVA, C_2H_4O with a molecular weight of 85,000–124,000 g/mol, ethanol, acetone, glass substrates, and parafilm oil were used. Deionized water was also utilized for the purposes of washing and sample preparation. It is essential to mention that the entire experiments were conducted at ambient temperatures.

B. Synthesis of Cu_2O NPs and Cu_2O/PVA Nanocomposites

A copper target of dimensions of 2×2 cm² and 3 mm thickness was used as the NP source. The target was ultrasonically cleaned for 15 min using acetone, ethanol, and deionized water to guarantee the elimination of impurities. After drying at ambient temperatures, the mass of the target was recorded as 7.0793 g. Cuprous oxide (Cu_2O) NPs were synthesized through a PLA method. The purified copper target was positioned in a cylindrical glass beaker containing 15 mL of deionized water at ambient temperature. The water level over the designated surface was calibrated to 0.5 cm by using a small glass cylinder as a foundation. An Nd: YAG laser (λ = 1064 nm, Q-switched) was used, operating at a fluence of 220 J/cm^2. Previous studies have shown that water level markedly attenuates laser power at 1064 nm while producing negligible attenuation at 532 nm (Hamad, Li and Liu, 2016). Consistent with those reports, we observed an approximate 13% reduction in laser power at a 0.5 cm water depth, which is attributable to the water's relatively high absorption coefficient at 1064 nm. In addition, the repetition rate was 5 Hz and the focal length was 5 cm. Different pulse counts of 250, 500, 750, 1000, 1250, and 1500 pulses were used to vaporize the target in deionized water. These pulse counts corresponded to six different mass concentrations of Cu_2O (0.01, 0.02, 0.027, 0.04, 0.05, and 0.063 mg/mL). Throughout the ablation procedure, the beaker and target stage were manually rotated to avert laser entrapment within cavities created on the target surface. A high-energy laser beam hits a metal target submerged in liquid and produces a superheated plume of plasma on the surface. The shock waves and the liquid pressure make this plasma expand rapidly in all directions. When it does cool, the plasma releases its thermal energy to the surrounding fluid, producing a cavitation bubble. As this bubble collapses, it generates a secondary shockwave and deposits NPs. The ablation resulted in the creation of copper NPs that oxidized when exposed to ambient oxygen, leading to the formation of Cu_2O NPs. The solution gradually changed from clear to pale green, indicating NP formation, as shown in Fig. 1a. The mass of the copper target was re-evaluated following the ablation process.

Nanocomposite, which includes PVA and Cu_2O was synthesized using the PLA process. A 4 % PVA solution was prepared by dissolving 4 g of PVA in 100 ml of deionized water, followed by continuous stirring for 2 hours at 68 °C to obtain a homogeneous and viscous solution. The same Nd: YAG laser settings were used to remove the copper target. Laser ablation was conducted in the PVA solution with pulse counts of 250, 500, 750, 1000, 1250, and 1500 following a consistent process. Using this method, Cu_2O NPs were spread out inside the PVA matrix, producing a Cu_2O/PVA nanocomposite. Fig. 1b shows a schematic diagram of the experimental setup of NPs and/or nanocomposite synthesis by the laser ablation technique.

III. Results and Discussion

A. X-ray Fluorescence (XRF)

XRF is a widely used technique to identify the elemental composition of materials, including copper targets. This method involves the irradiation of high-energy X-rays onto a sample, resulting in the emission of secondary X-rays that are unique to the different elements within the sample. XRF analyzes the emitted X-ray and provides identification and quantitation of elements with an atomic number from 11 (sodium) and beyond 92 (uranium) and from parts per million (ppm) to 100%. XRF spectroscopy is an excellent and non-destructive technique for validation of the purity and elemental constituents of the copper target utilized to synthesize materials (González, Saadatkhah and Patience et al., 2024). Cu target was examined by means of XRF of type Rigaku, NEXCG, and the analysis showed no significant impurities, which is an essential condition in areas requiring pure copper and nanocomposite preparation (Marguí, Queralt and De Almeida, 2022). Table 1 shows the XRF data confirming the purity of the copper target.

B. NP Concentration in Deionized Water

The amount of ablated material was weight-based; a four-decimal-place highly-sensitive balance (Max 210 g, d = 0.1 mg) was used for this purpose. This procedure involves weighing the target before and after ablation. The procedure was replicated for each number of laser pulses. Drying of the target was done after ablation, before the final weight was recorded. The mass ablated (ΔM) was subsequently computed as below:

$$\Delta M = m_b - m_a \quad (1)$$

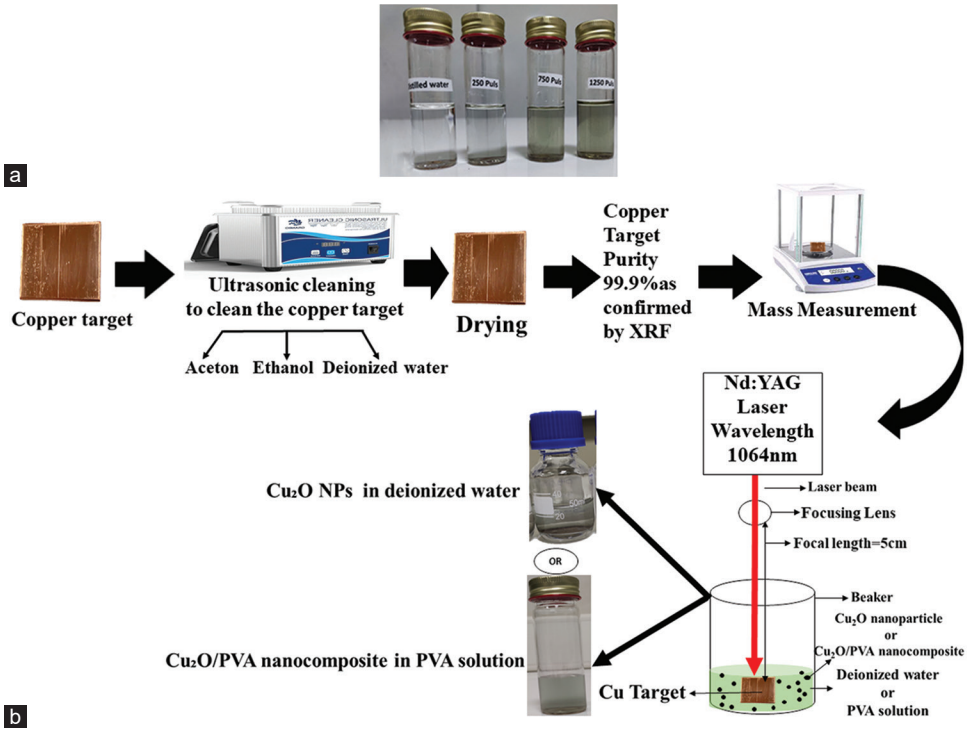

Fig. 1. (a) Formation of Cu_2O NPs. (b) Experimental setup of nanoparticles (NPs) and/or nanocomposite synthesis by laser ablation technique

Where m_b is the target mass before the ablation process and m_a is the target mass after the ablation process. The mass concentration, on the other hand, can be calculated as follows:

$$\text{Mass concentration} = \frac{\Delta M}{\text{liquid criterion}} \left(\frac{\text{mg}}{\text{ml}} \right) \quad (2)$$

C. Fourier Transform Infrared (FTIR) Spectroscopy Analysis

FTIR spectroscopy is utilized in the examination of various types of materials, including bulk materials, thin films, liquids, solids, pastes, powders, and fibers. Both qualitative identification of constituents with the aid of appropriate standards and quantitative analysis of their concentrations are provided by FTIR analysis (Tkachenko and Niedzielski, 2022). The FTIR of type Shimadzu IRAffinity-1S was conducted to find out how the PVA matrix and Cu_2O NPs might interact with each other and to find out what kinds of vibrational bands and functional groups are in the Cu_2O/PVA nanocomposite. Fig. 2 displays the FTIR spectra of PVA and Cu_2O/PVA nanocomposite (at 250, 500, and 1000 pulses).

The FTIR spectra of pure PVA and Cu_2O/PVA samples show different peaks that are linked to various functional groups and vibrational modes. O–H stretching (3300–3400 cm^{-1}) exhibited peaks at 3318 cm^{-1}, 3323 cm^{-1}, 3333 cm^{-1} and 3338 cm^{-1}. These peaks correspond to the O–H stretching vibrations in PVA. The alteration in peak position (from 3318 cm^{-1} in pure PVA to 3338 cm^{-1} in PVA with 1000 laser pulses) signifies hydrogen bonding between the hydroxyl groups in PVA and the Cu_2O NPs (Vijayashree, Rai and Demappa, 2016). As Cu_2O concentration increases,

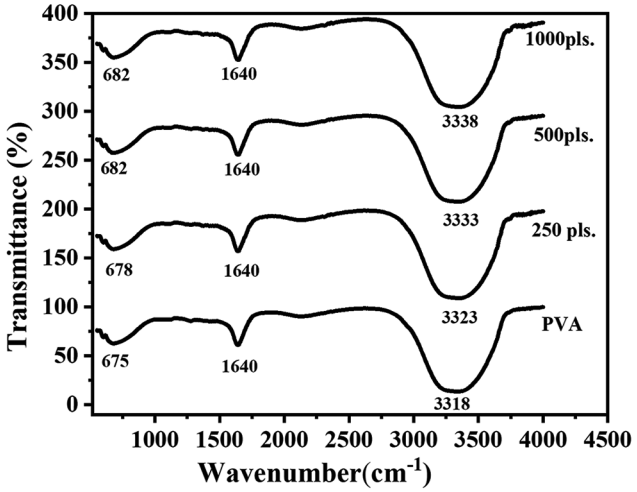

Fig. 2. Fourier transform infrared spectra of polyvinyl alcohol (PVA) and Cu_2O/PVA nanocomposites synthesized at 250, 500 and 1000 laser pulses

TABLE I
X-Ray Fluorescence (XRF) Data of the Cu Target

Elements	Concentration (%)	Counts-KA
Cu	99.9	2727020 Mo
Al	0.0858	1249 RX9
Si	0.0344	1720 RX9
Sn	0.0113	262 Al
P	0.0094	1517 RX9
S	0.0088	2093 RX9

the O-H stretching peak shifts toward higher wavenumbers, suggesting improved interaction between PVA hydroxyl groups and Cu_2O NPs. Although no new peaks were observed, the shifting of the present peaks indicates possible structural

modifications brought on by Cu_2O incorporation. According to the FTIR analysis, the main path that Cu_2O NPs interact with PVA is by forming hydrogen bonds with hydroxyl groups, which causes vibrational modes to shift. A well-dispersed composite is confirmed by the absorption bands and their shifts, which show structural alterations, while the PVA matrix keeps its functional groups. Cu_2O/PVA is appropriate for important applications because of these interactions, which improve the material's qualities. Furthermore, C=O stretching (1717–1742 cm^{-1}) observed a peak at 1640 cm^{-1} for all samples. This peak signifies the vibrational stretching of carbonyl (C=O) groups in PVA or C=C stretching, especially if there are oxidative modifications or secondary interactions happening in the matrix. The stable position of this peak shows that the carbonyl environment is not changed much, while Cu_2O may have some small interactions with these groups. This band is usually attributed to the H–O–H bending vibration of adsorbed water molecules in the PVA matrix or on the surface of CuO NPs (El-Ghoul, et al., 2021, Manjunath, et al., 2016). The C–C and $–CH_2$ vibrational modes (818–833 cm^{-1}), on the other hand, show peaks at 675 cm^{-1} in pure PVA, 678 cm^{-1} in PVA that has been exposed to 250 laser pulses, and 682 cm^{-1} in PVA that has been exposed to both 500 and 1000 laser pulses. The peaks are displaced, but may indicate the $–CH_2$ vibrations or C–C stretching modes in PVA. The alteration in this region is likely attributable to the incorporation of Cu_2O, which modifies the molecular environment of PVA (Aslam, Raza and Siddique, 2021b). C–H asymmetric stretching (2923–2948 cm^{-1}) identified in the 2900–3000 cm^{-1} range is wide but not distinctly marked. This region pertains to the asymmetric stretching of aliphatic C–H bonds within the PVA backbone (Eid, 2022, Kanchana, et al., 2023b). C–H bending and wagging occur at 1370–1389 cm^{-1} and 1243–1226 cm^{-1}, with potential peaks (not labeled) at 1370–1389 cm^{-1}. The C-H bonds undergo bending vibrations at 1226–1243 cm^{-1} and $–CH_2$ wagging vibrations in PVA. The modes are affected by the interaction between Cu_2O NPs and the PVA matrix (Kanchana. et al., 2023b). In the range of 1094–1100 cm^{-1}, vibrational stretching of C–O and C–O–C bonds happens with potential peaks in the range of 1000–1100 cm^{-1} for the acetyl groups in PVA (Liu and Kazarian, 2022). No additional peaks were observed; however, a subtle shift in this region indicates an interaction between Cu_2O and the hydroxyl groups in PVA.

D. X-ray Diffraction (XRD) Analysis

The powder XRD pattern of the prepared samples was obtained using the Explorer XRD system of copper Kα x-rays of wavelength (λ = 1.540598 Å). The samples obtained were scanned between 5 and 80 degrees with a step size of 0.010. Fig. 3a and b shows XRD spectra of synthesized Cu_2O NPs and Cu_2O/PVA nanocomposite at 1000 pulses, respectively. As can be seen in Fig. 3a, the peak positions are in good agreement with those of Cu_2O powder obtained from the International Center of Diffraction Data card (JCPDS file no. 05-0667) conforming the formation of cubic crystal structure with the unit cell 4 Journal Pre-proof parameters (a = b = c = 4.269 Å) (Ramesh, et al., 2012, Fazio, et al., 2020, Zhou, et al., 2025, Zhang, et al., 2007, Mostafa, et al., 2019). The peaks with 2θ values of 29.53°, 36.4°, 42.27°, 61.30°, and 73.47° correspond to the crystal planes of 110, 111, 200, 220, and 311 of crystalline Cu_2O, respectively. These peaks specifically at 2θ ≈ 36.4° (111) and 42.27° (200), indicating the formation of a pure Cu_2O phase (Raship, et al., 2017, Ahmed, Sabri and Mohammad, 2020, Husham, et al., 2024). Moreover, a low-angle feature at ≈ 8.0° indicates the presence of a lamellar/intercalated phase (e.g., a hydrated layered copper species or ordered adsorbed layer). Fig. 3b showed a peak at approximately 2θ = 19.74° corresponding to (101) crystal plane for PVA, which indicates the semi-crystalline nature of PVA. The crystalline nature of PVA results from the strong intermolecular interaction between PVA chains through hydrogen bonding. The PVA helps with the uniform dispersion of Cu_2O NPs due to plenty of hydroxyl groups present on its backbone (Rao, et al., 2015). In addition, it was observed that the position of the PVA reflection peak at 19.74° does not significantly affected by the incorporation of copper NPs, indicating the good dispersion of Cu_2O nanofiller in the PVA matrix (Fazio, et al., 2020, Manjunath, et al., 2016, Xiao, 2012, Qian, et al., 2001). The Cu_2O diffraction peak is obscured by the PVA matrix, which suggests that PVA has precipitated inside or within the Cu_2O NP, thereby masking the Cu_2O signal. In other words, the XRD pattern of the Cu_2O/PVA nanocomposites is dominated

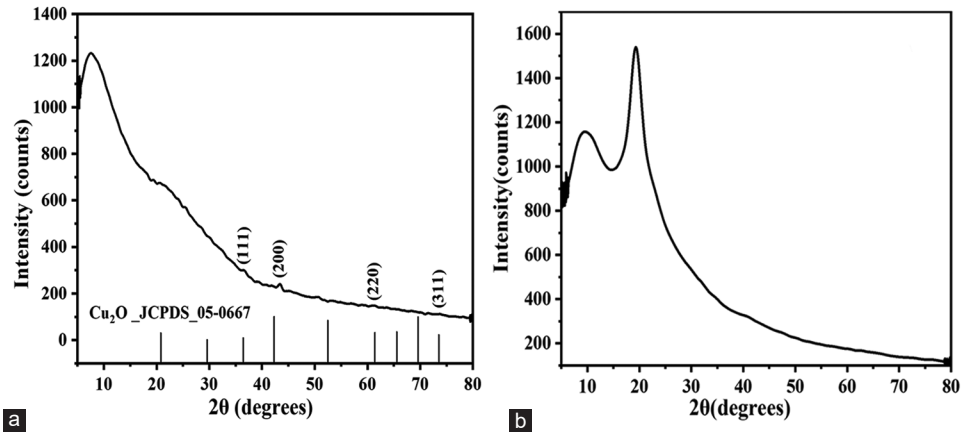

Fig. 3. The X-ray diffraction spectra of (a) synthesized Cu_2O nanoparticles and (b) Cu_2O/polyvinyl alcohol nanocomposites at 1000 laser pulses

by the amorphous PVA halo centered at ≈ 19.7°. These results confirm that metal ions (cupric ions) are reduced to crystalline Cu_2O particles embedded in a PVA matrix due to the effect of the high intensity of PLA process (Menazea, Mostafa and Al-Ashkar, 2020). The diffraction line at 2θ ≈ 52.5° listed in JCPDS card 05-0667 may be absent in the measured pattern for two main reasons. First, that reflection is intrinsically weak and can fall below the instrument noise when the Cu_2O phase fraction is low or the crystallites are very small. Second, a strong preferred orientation (texture) in the thin film can suppress diffraction from the plane that produces the 52.5° peak (Holder and Schaak, 2019).

E. Dynamic Light Scattering (DLS) Analysis

DLS of type Mastersizer 3000 Malvern was used to determine the particle size distribution of the synthesized Cu_2O NPs. The size distribution histograms of 750 pulses in deionized water showed that the size of the Cu_2O NPs ranged from ~0.7 μm to ~1.4 μm with a mean distribution diameter of ~ 1.0 μm and from ~ 2.6 μm to ~3.7 μm with an average of ~3.1 μm for the same Cu_2O NPs as depicted in Fig. 4a. The DLS showed the presence of NP agglomeration, which revealed the uniformity of the Cu_2O NPs. The DLS studies revealed polydispersity of Cu_2O NPs. This indicates that the initial stages of NP formation were achieved, but significant agglomeration occurred in the absence of a stabilizing agent. The outermost layer can absorb water, producing tumescence of the composite NPs and, as a result, increasing particle sizes. The influence of particle concentration in a solution becomes more pronounced when the particles are unstable and prone to aggregation. In such cases, the main source of error is not multiple scattering, but the increased size of the resulting conglomerates. Consequently, as the substance concentration rises, the particle sizes measured by DLS will appear larger (Yeap, et al., 2018). The DLS technique is unable to distinguish NPs whose sizes differ by less than a factor of three. For instance, a 1:1:1 mixture of latex NPs with diameters of 220, 330, and 440 nm would appear as a single broad peak in the size distribution. Aggregation in such systems may result from factors, such as high particle concentration, surface charge interactions in the solution, or the presence of unfiltered particulates. Even small amounts of aggregates can significantly distort DLS measurement results (Filippov, et al., 2023). On the other hand, the size distribution histograms for 750 pulses within PVA solution showed that the size of the Cu_2O/PVA nanocomposites ranged from ~ 20 nm to ~ 1.7 μm with a mean distribution diameter of ~ 800 nm and from ~ 2.2 μm to ~ 3.9 μm with an average of ~ 3 μm for the same Cu_2O NPs as illustrated in Fig. 4b. The DLS findings of Cu_2O NPs synthesized within PVA solution indicate the improved size control and colloidal stability due to the polymer's stabilizing features (Ghosh, et al., 2024). In general, because DLS is more sensitive to larger particles, the scattering intensity scales with the sixth power of particle radius. As a result, even at much lower concentrations, larger particles can overshadow the signal from smaller particles, which may be far more abundant in the solution. Employing volume- and number-weighted distribution functions can aid in detecting and characterizing these smaller particles (Casillo, et al., 2021).

F. Optical Characterization

Ultraviolet-visible (UV-Vis) spectroscopy

The UV–Vis (of type Cary Series [100] UV-Vis Spectrophotometer) absorption spectra of Cu_2O NPs at 25°C are shown in Fig. 5. The ranges shown in the figure are generally encompasses the UV to visible light spectrum and they are essential for the analysis of semiconductor materials, such as Cu_2O (Aslam, Kalyar and Raza, 2021a). Strong absorbance was observed between 240 and 360 nm, which means that the Cu_2O NPs are going through strong electronic transitions. This aligns with data indicating that Cu_2O displays distinctive absorbance in this range due to band-to-band transitions. As concentration increases, absorbance similarly rises, indicating that higher concentrations lead to more electronic transitions and enhanced light absorption (Kanchana, et al., 2023b). The absorbance decreases following the peak, which is characteristic of semiconductor materials. This indicates that beyond a specific wavelength, the material exhibits ineffective light absorption, reflecting its optical characteristics. The UV-Vis shows that the Cu_2O NPs behave as typical semiconductors, with absorption peaks that

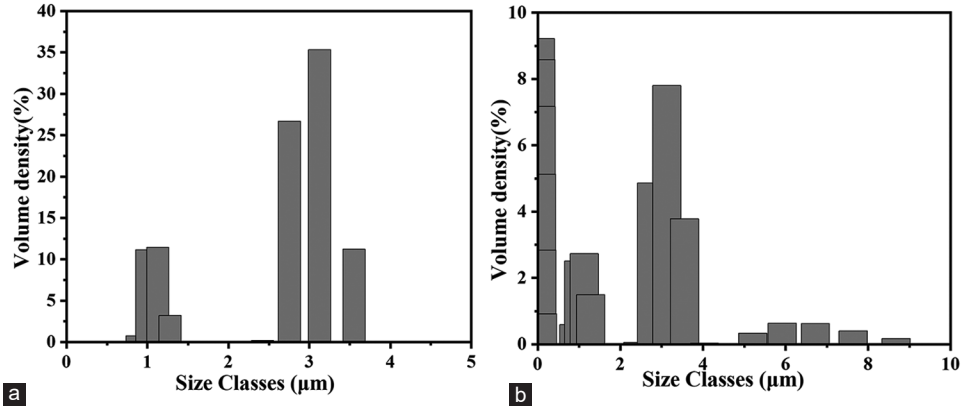

Fig. 4. Dynamic light scattering histograms of the size distribution of Cu_2O nanoparticles in (a) deionized water and (b) polyvinyl alcohol solution at 750 laser pulses

http://dx.doi.org/10.14500/aro.12222

change with concentration and clear electronic transitions in the UV range. These findings may have ramifications for applications in photocatalysis and solar energy (Singh, et al., 2023). In addition, Fig. 5 exhibits significant absorption in the UV region (below about 400 nm), which is an indication of Cu_2O NPs. The absorbance beyond around 400 nm diminishes, signifying a decreased interaction with visible light. As the number of laser pulses escalates from 250 to 1500, the intensity of the absorption peaks varies. The spectrum for 1500 pulses exhibits a distinct absorption peak near 320 nm, perhaps attributable to particular NP aggregation or structural alterations. The trend demonstrates that the concentration or morphology of NPs is substantially influenced by the number of laser pulses. Since Cu_2O NPs do not absorb much at wavelengths above 500 nm, this means that they mostly absorb in the UV range, which is in the line with how they look.

UV -visible absorption spectra for the resulting Cu_2O NPs from PLA with pulse laser settings varying from 250 to 1500 PLS show wide absorption bands for wavelengths between 240 and 360 nm, corresponding to the surface plasmonic resonance (SPR) for Cu_2O. SPR's strength is found to rise with an increasing number of laser pulses, corresponding to an increase in the amount of NPs generated. In addition, the SPR peak is found to redshift with increasing PLS, indicating the particles are increasing and becoming aggregated. On the other hand, in those with lower PLS, NPs are found to represent smaller sizes along with finer spatial distribution. These results demonstrate that the number of laser pulses presented can profoundly affect the NPs' size, in addition to the optical properties, and support earlier findings concerning the SPR for Cu_2O (Alruwaili, et al., 2025).

Fig. 6 shows that the highest absorbance intensity is in the UV range (about 200–400 nm), which means that Cu_2O NPs absorb a lot of light in this range. The absorption edge of Cu_2O/PVA samples was detected in the region of around 250–335 nm. The absorption edge of the Cu_2O/PVA nanocomposites shifted to the red, showing that the optical band gap of PVA can be changed by very small amounts of NPs. The redshift of the absorption edge in the samples showed that the Cu_2O NPs and the –OH groups of the PVA were hydrogen-bonded, as confirmed also from FTIR analysis. The connections between the matrix and NPs are caused by changes in the crystallinity of the matrix, which in turn are caused by changes in the synthesized samples' band gaps (Aslam, Kalyar and Raza, 2021a). The peaks are pronounced at lower wavelengths and tend to increase as the wavelength increases. An increase in the number of laser pulses results in heightened absorption intensity, especially evident in the UV spectrum. By increasing the number of pulses, the concentration of Cu_2O NPs increases. This is due to the fact that the ablation process is better. The uniform absorbance patterns indicate stabilization by the PVA matrix, inhibiting NP agglomeration. The 1500-pulse spectrum demonstrates the maximum absorption and correlating with increased NP production. Beyond 400 nm, the absorbance considerably decreases, exhibiting a plateau. In the visible spectrum, this means that the Cu_2O NPs embedded in the

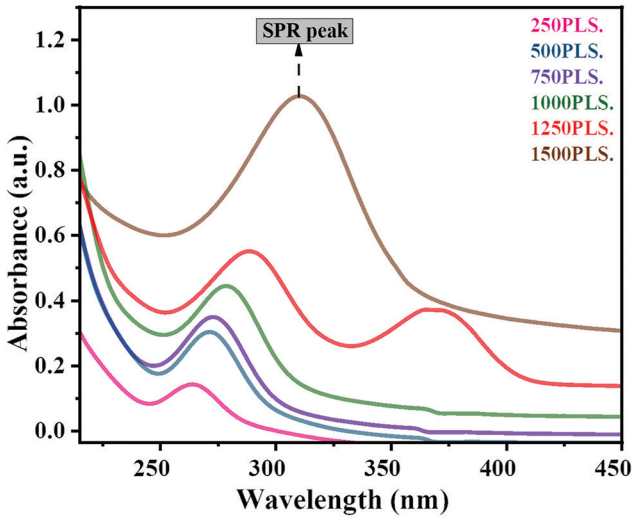

Fig. 5. Ultraviolet-visible spectroscopy data of Cu_2O nanoparticles synthesized in deionized water at 250, 500, 750, 1000, 1250 and 1500 of laser pulses, respectively

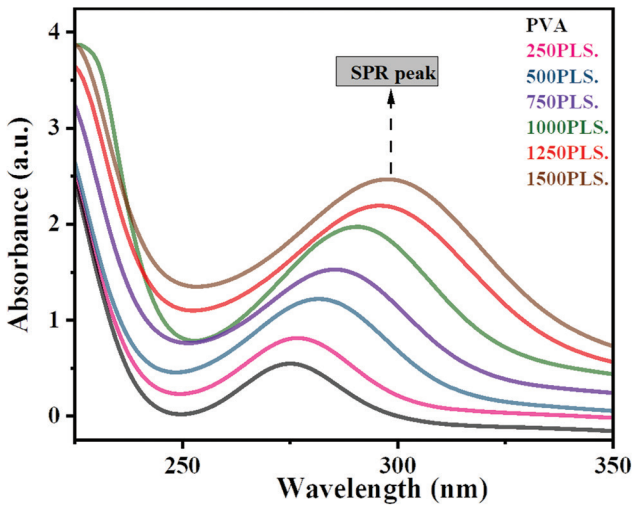

Fig. 6. Ultraviolet-visible spectroscopy data of polyvinyl alcohol (PVA) and Cu_2O/PVA nanocomposite synthesized in PVA solution at 250, 500, 750, 1000, 1250 and 1500 of laser pulses, respectively

PVA matrix are optically clear. The absorbance characteristics of the PVA matrix validate its function in stabilizing the Cu_2O NPs and inhibiting aggregation. The pure PVA film displays an absence of absorption peaks for the visible region; hence, the confirmation for the optical transparency. The Cu_2O/PVA nanocomposites; however, exhibit a broad absorption band over 250–340 nm, in which the characteristic of the SPR corresponding to the Cu_2O NPs.

At lower pulse counts (250–500 PLS), as shown in Fig. 6, the comparatively weak blue-shifted SPR band suggests the existence of energetically dispersed, smaller-sized Cu_2O NPs. Conversely, at higher pulse counts (1000–1500 PLS), the intensified and red-shifted SPR peak suggests the formation of larger or more aggregated particles. Such an observation is meant to reveal that the optical performance of Cu_2O NPs is exactly tunable with the change in the number of laser

pulses. The main difference between Figs. 5 and 6 is that the absorbance of the Cu_2O/PVA nanocomposites is significantly higher than that of the Cu_2O NPs.

SPR is produced due to the collective oscillation of the conduction band electrons at the surface of NPs under the action of incoming light. The exact position and strength of this SPR band are functions of numerous variables, namely, particle size and morphology, and the dielectric constant of the medium surrounding the particles, specifically the PVA matrix. When the number of laser pulses is raised, the SPR peak is intensified and shifts to longer wavelengths, indicating an increase in the particle size and an increase in particle density due to increased ablation and deposition under the pulsed laser process.

Observation of a clear SPR band is strong evidence for the successful synthesis of Cu_2O NPs in the PVA matrix through the *in situ* process and demonstrates the effect of the laser processing parameters on the optical behavior (Han, et al., 2021).

Tauc plots of Cu_2O and Cu_2O/PVA nanocomposite

The optical bandgap of Cu_2O NPs was determined by extrapolating the linear region of the Tauc plot near the absorption edge. To gain a deeper understanding of the observed optical properties, we calculated the optical energy gap (E_g) of PVA and Cu_2O/PVA nanocomposites using the Tauc equation as follows:

$$(\alpha E)^n = B\,(E\text{-}E_g) \quad (3)$$

Where E denotes photon energy, α represents the absorption coefficient, B is a constant, and E_g indicates the band gap energy. Furthermore, n = 2 for the indirect bandgap and n = 1/2 for the direct bandgap. Thus, Tauc plots for direct bandgap can be constructed and the extrapolations of the graph's significant x-axis, where the y-axis value equals zero. E_g can be determined from this plot as demonstrated in Figs. 7 and 8, and summarized in Table 2. Fig. 7 shows different curves of the optical properties of Cu_2O NPs that were made by using different amounts of laser pulses. For example, 250 pulses indicate a higher band gap, suggesting smaller particles due to quantum confinement (Kambhampati, 2021, Qiao and Son, 2021). A more pronounced slope indicates greater particle sizes and a reduced band gap at 500 pulses. In 750 pulses, the gradient keeps going down, which probably means that the NPs are getting bigger and more uniform, which lowers the band gap, and at 1000 pulses, the curve indicates optimized particle size, potentially stabilizing the band gap. Finally, the curves at 1250 and 1500 pulses are very steep, which suggests that the changes in optical properties have reached a stable band gap energy because the NPs have gathered together. As the number of laser pulses escalates, the band gap shifts, probably due to differences in particle size, morphology, and crystallinity.

Aggregation of NPs can alter the absorption spectra by affecting the effective density of states. Strong light scattering, especially in particles that are spread out in many different directions, can change the Tauc plot, making the bandgap getting bigger. Cu_2O NPs made by laser ablation have high surface-to-volume ratios, which cause stress and strain inside the particles. These structural alterations modify the electronic band structure, frequently resulting in an apparent increase in the bandgap (Kudhur, et al., 2024, Mallik et al., 2020). The higher bandgap values found in the Tauc plot for Cu_2O NPs made by laser ablation in deionized water can be explained by some factors, such as the size of the NPs, quantum confinement effects, defect states, oxygen vacancies, lattice strain effects, and light scattering.

Fig. 8 shows the Tauc curves for virgin PVA and for Cu_2O/PVA nanocomposites synthesized in a PVA solution with various amounts of laser pulses of 250, 500, 750, 1000, 1250, and 1500. The determined band gap value for virgin PVA was 5.00 eV, as indicated by Fig. 8. This should show little to no absorption in the visible range, indicating its insulating nature. At 250 pulses, the slope is very gentle, indicating a relatively smaller band gap. However, it could also be due to the PVA concentration being higher and/or the NP concentration being lower, in addition to the NP not being very homogeneous in the PVA matrix. At 500 pulses, an increase in slope; indicating a potential increase in NP concentration and a decrease in band gap energy. The probable reason is that Cu_2O NPs are more dispersed in the PVA matrices. The slope continues to increase, indicating that the NPs are dispersing more widely in the PVA and are becoming increasingly crystallized, thus lowering the band

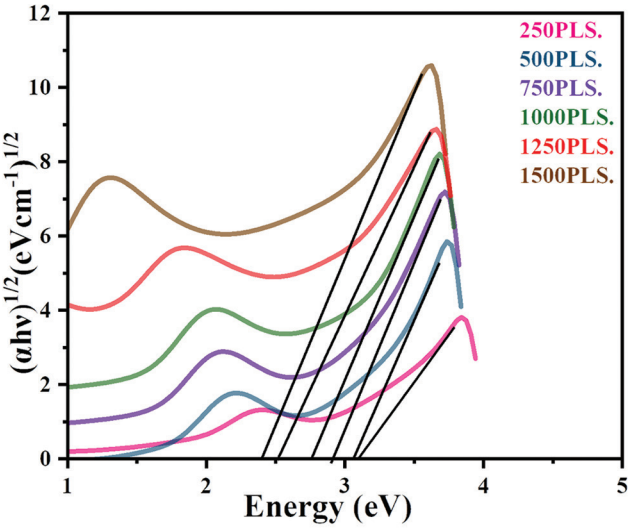

Fig. 7. Tauc's plot data of Cu_2O nanoparticles synthesized in deionized water at 250, 500, 750, 1000, 1250 and 1500 of laser pulses, respectively

TABLE II
THE CALCULATED BANDGAP OF Cu_2O AND Cu_2O/PVA NANOCOMPOSITES SYNTHESIZED IN DEIONIZED WATER AND IN PVA SOLUTION FOR DIFFERENT NUMBER OF LASER PULSES

Laser pulses	Cu_2O (eV)	Cu_2O/PVA (eV)
250	3.1	4.63
500	3.06	4.29
750	2.91	4.02
1000	2.76	3.79
1250	2.51	3.51
1500	2.4	3.14

http://dx.doi.org/10.14500/aro.12222

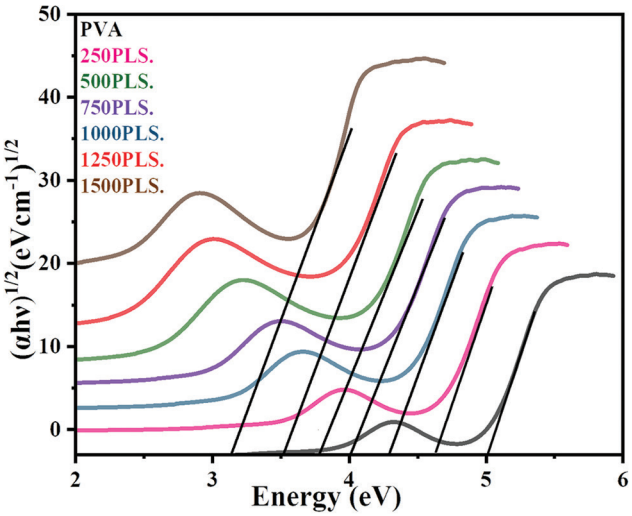

Fig. 8. Tauc's plot data of polyvinyl alcohol (PVA) and Cu_2O/PVA nanocomposite synthesized in PVA solution at 250, 500, 750, 1000, 1250 and 1500 of laser pulses, respectively

gap at 750, 1000, 1250, and 1500 pulses; this curve is the most favorable scenario for particle size and distribution, which can stabilize the band gap.

As the number of laser pulses increases, a reduction in band gap energy is observed, which can be attributed to the increased concentration of NPs within PVA matrices. This reduction is due to the interaction between the PVA and Cu_2O NPs. This introduces new energy states and narrows the gap between the valence and conduction bands. These results are consistent with other findings (Abdullah, et al., 2015); (Singh, et al., 2023); (Aslam, Kalyar and Raza, 2021a) (Kanchana, Vanitha and Basavaraj, 2023a). The presence of PVA as a matrix can affect the dispersion, stability, and optical properties of the Cu_2O NPs. The interaction between Cu_2O and PVA may also affect the band gap. The polymer matrix may stabilize the NPs, thereby improving optical performance.

Photoluminescence (PL) analysis

Photoluminescence (PL) is a method that evaluates the electronic structure influenced by the complex particle sizes arising from crystallinity (Alzahrani, 2022). The PL (of type Cary Eclipse Fluorescence Spectrophotometer, G9800A) spectrum of the obtained samples, using the excitation wavelength of 300 nm, reveals an emission band around 600–601.5 nm across all synthesized NPs in both deionized water and PVA solutions. This persistent emission band confirms the formation of the Cu_2O phase. The peak intensity escalates with the concentration of the solution, signifying a correlation between concentration and measured intensity. The peak emission at 600–601.5 nm is caused by the recombination of direct excitons (X_0-line) without phonons participation, which represents the band gap emission of Cu_2O. The strong band gap emission shows that the cuprous oxide thin layer that formed has better crystalline quality (David Prabu, et al., 2018).

The PL spectra of Cu_2O acquired with an excitation wavelength of 300 nm are presented in Fig. 9. The figure exhibits a pronounced peak in intensity within the designated wavelength range, indicating a robust emission or absorption characteristic at that wavelength. As the pulses escalate, the strength of the peaks seems to fluctuate, suggesting a correlation between the number of pulses and the recorded intensity. Furthermore, it signifies an elevated concentration or enhanced crystallinity of Cu_2O NPs in the samples. The peak at 1500 pulses appears to be the most significant. The lines representing various well-aligned pulse counts indicating that the measurements are consistent between trials with minor fluctuations in peak intensity. This corresponds to the anticipated behavior, as an increased number of pulses would produce a larger volume of NPs. All of the spectra show a main peak between 600 and 601.5 nm, which is typical of Cu_2O NPs and is caused by their bandgap transitions or defect states. Minimal spectral broadening indicates a generally homogeneous NP size distribution across varying pulse counts. The pattern indicates that after 1500 pulses, the peak intensity may start to saturate or stabilize, potentially signifying a limit to NP concentration or reabsorption. The stronger laser pulses mean that quantum confinement effects are stronger or that the optical properties are better because particles are dispersed or more effectively synthesized. The uniformity in the emission wavelength indicates little variation in particle size or defect state among different laser pulses (Xu, et al., 2018, Aslam, Kalyar and Raza, 2017).

The PL spectrum of the synthesized Cu_2O/PVA nanocomposite, utilizing an excitation wavelength of 300 nm, is depicted in Fig. 10. The graph indicates a significant emission peak at around 600 nm for all samples generated with different Cu_2O concentrations. This constant peak signifies a sustained photoluminescent response across many sample preparations. This means that the PL abilities get better as Cu_2O content rises. This trend indicates that the Cu_2O/PVA nanocomposite could create and more effectively combine exciton. The dominant feature at 600 nm is assigned to direct exciton recombination akin to the X_0 line of Cu_2O. This indicates that the phonon interaction does not contribute to luminescence, which is characteristic of highly pure and crystallized samples. The emission of this small band gap at 600 nm indicates that the Cu_2O/PVA nanocomposite possessed suitable crystal quality. This is significant for the utilization of the material in optoelectronic devices since, typically, efficient light emission accompanies the crystalline quality of the material. The emission band appearing at 600 nm confirms the formation of Cu_2O phase in the nanocomposite. Higher Cu_2O concentrations may contribute to the increase in peak intensity, where improved exciton mobility and reduced non-radiative recombination led to more efficient light emission. These features highlight the significance of material crystallinity, as increased crystallinity generally correlates with superior electrical properties and improved luminescence behavior (David Prabu, et al., 2018).

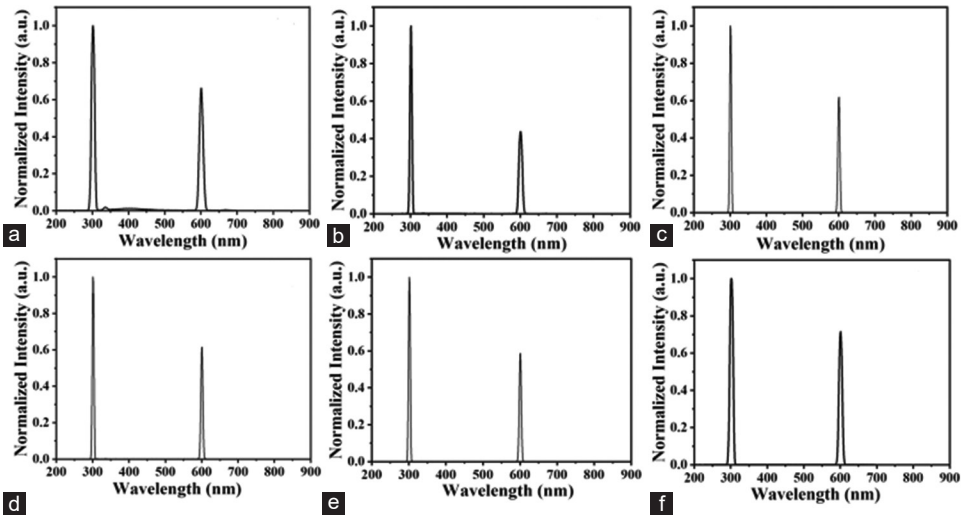

Fig. 9. (a-f) Photoluminescence spectroscopy data of Cu_2O nanoparticles at 250, 500, 750, 1000, 1250 and 1500 laser pulses, respectively

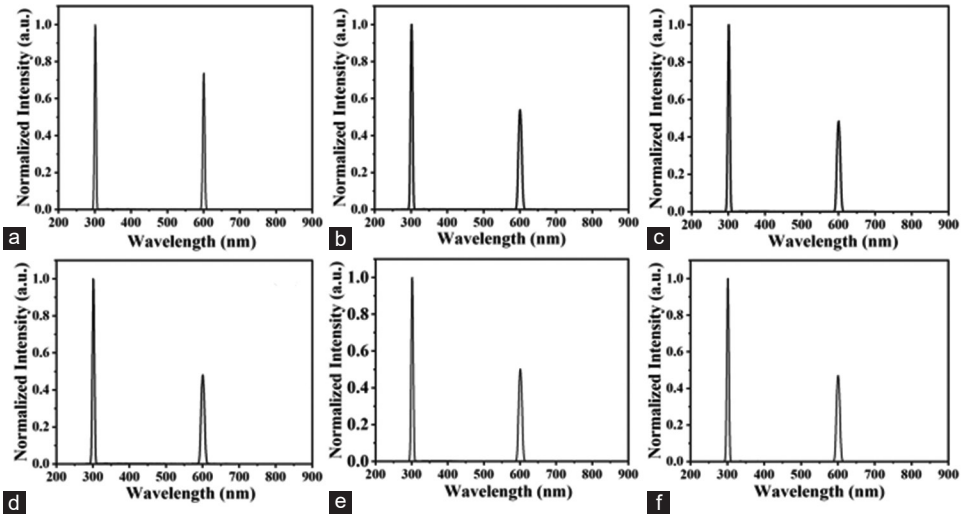

Fig. 10. (a-f) Photoluminescence spectroscopy data of Cu_2O/polyvinyl alcohol nanocomposite at 250, 500, 750, 1000, 1250 and 1500 laser pulses, respectively

IV. Conclusion

This study reports the successful synthesis and characterization of PVA nanocomposites doped with different mass concentrations of Cu_2O NPs using laser ablation. The synthesized nanocomposites were analyzed and compared to Cu_2O NPs of identical mass concentrations using XRD, DLS, UV-vis spectroscopy, PL spectroscopy, and FTIR. XRD confirms the existence of Cu_2O phase NPs. The DLS showed the presence of NP agglomeration, which revealed polydispersity of Cu_2O NPs. The FTIR results show that Cu_2O NPs mostly interact with PVA by hydrogen bonding with hydroxyl groups, which changes the vibrational modes. Furthermore, the UV-vis study shows that the Cu_2O NPs behave like normal semiconductors, with absorption peaks that change depending on the concentration and clear electronic transitions in the UV region. These findings can have implications for applications in photocatalysis and solar energy. The determined band gap value for virgin PVA was 5.00 eV, as indicated by UV-vis spectroscopy. As the concentration of Cu_2O rises, the band gap significantly narrows, highlighting significant alterations in the electronic structure of the PVA matrix. The uniform absorbance patterns indicate stabilization by the PVA matrix, inhibiting NPs agglomeration. The Tauc plots showed that adding NPs changes the optical band gap, which decreases as the mass concentration of Cu_2O increases. The anomalously elevated bandgap values of Cu_2O NPs as determined by the Tauc plot can be ascribed to many reasons, such as NP size, quantum confinement effects, defect states, oxygen vacancies, lattice strain effects, and light scattering. From PL, minimal spectral broadening indicates a generally homogeneous NP size distribution across varying pulse counts. These results show that the optical properties of Cu_2O/PVA nanocomposites can be tailored for various state-of-the-art applications, laying out the grounds of laser ablation as an efficient synthetic method for high-quality nanostructures.

References

Abdelfatah, M., Darwesh, N., Habib, M.A., Alduaij, O.K., El-Shaer, A., and Ismail, W., 2023. Enhancement of structural, optical and photoelectrochemical properties of n- Cu_2O thin films with k ions doping toward biosensor and solar cell applications. *Nanomaterials (Basel)*, 13, p.1272.

Abdullah, O.G., Aziz, S.B., Omer, K.M., and Salih, Y.M., 2015. Reducing the optical band gap of polyvinyl alcohol (PVA) based nanocomposite. *Journal of Materials Science: Materials in Electronics,* 26, pp.5303-5309.

Abdulnabi, G., and Juda, A.M., 2023. Preparation and comparison performance of CuO Nanopartecles and CuO/TiO2/Nanocomposite and application in solar cell. *Journal of Kufa-Physics*, 15, pp.1-13.

Ahmed, M.A., Sabri, M.M., and Mohammad, H.Q., 2020. Study of structural and optical properties of Cu_2O thin film prepared by rapid thermal annealing using Nd-YAG laser. *NeuroQuantology,* 18, pp.15-22.

Al-Hakimi, A.N., Asnag, G., Alminderej, F., Alhagri, I.A., Al-Hazmy, S.M., and Qahtan, T.F., 2023. Enhancing the structural, optical, thermal, and electrical properties of PVA filled with mixed nanoparticles (TiO2/Cu). *Crystals*, 13, p.135.

Alruwaili, A., Gamal, H., Alziyadi, M.O., Alkabsh, A., Alawi, M.J., and Shalaby, M.S.A., 2025. Engineered nanoparticle doping, structural, and optical innovations in polyvinyl alcohol composites for advanced optoelectronic applications. *Journal of Thermoplastic Composite Materials*, 38, p. 4012-4056.

Alzahrani, H.A., 2022. CuO and MWCNTs nanoparticles filled PVA-PVP nanocomposites: Morphological, optical, dielectric, and electrical characteristics. In: *Carbon Nanotubes-Recent Advances, New Perspectives and Potential Applications.* IntechOpen, London.

Aslam, M., Kalyar, M.A., and Raza, Z.A., 2017. Fabrication of reduced graphene oxide nanosheets doped PVA composite films for tailoring their opto-mechanical properties. *Applied Physics A*, 123, pp.1-12.

Aslam, M., Kalyar, M.A., and Raza, Z.A., 2021a. Fabrication of nano-CuO-loaded PVA composite films with enhanced optomechanical properties. *Polymer Bulletin*, 78, pp.1551-1571.

Aslam, M., Raza, Z.A., and Siddique, A., 2021b. Fabrication and chemo-physical characterization of CuO/chitosan nanocomposite-mediated tricomponent PVA films. *Polymer Bulletin*, 78, pp.1955-1965.

Awal, R., Tanisa, N.Y., Rahman, M.A., and Ahmed, S., 2024. Preparation of nanostructured cuprous oxide (Cu_2O) absorber layer for photovoltaic application. *Micro and Nano Letters*, 19, p.e12188.

Aziz, S.M.A., Nayef, U.M., and Rasheed, M., 2025. Synthesis of copper oxide nanoparticles via laser ablation in liquid for enhancing spectral responsivity. *Plasmonics,* 20, pp.2869-2879.

Casillo, A., Fabozzi, A., Russo Krauss, I., Parrilli, E., Biggs, C.I., Gibson, M.I., Lanzetta, R., Appavou, M.S., Radulescu, A., and Tutino, M.L., 2021. Physicochemical approach to understanding the structure, conformation, and activity of mannan polysaccharides. *Biomacromolecules,* 22, pp.1445-1457.

David Prabu, R., Valanarasu, S., Ganesh, V., Shkir, M., Alfaify, S., and Kathalingam, A., 2018. Investigation of molar concentration effect on structural, optical, electrical, and photovoltaic properties of spray-coated Cu_2O thin films. *Surface and Interface Analysis*, 50, pp.346-353.

Eid, M.M., 2022. Characterization of nanoparticles by FTIR and FTIR-microscopy. In: *Handbook of Consumer Nanoproducts.* Springer, Germany.

El-Ghoul, Y., Alminderej, F.M., Alsubaie, F.M., Alrasheed, R., and Almousa, N.H., 2021. Recent advances in functional polymer materials for energy, water, and biomedical applications: A review. *Polymers*, 13, p.4327.

Fazio, E., Gökce, B., De Giacomo, A., Meneghetti, M., Compagnini, G., Tommasini, M., Waag, F., Lucotti, A., Zanchi, C.G., and Ossi, P.M., 2020. Nanoparticles engineering by pulsed laser ablation in liquids: Concepts and applications. *Nanomaterials*, 10, p.2317.

Filippov, S.K., Khusnutdinov, R., Murmiliuk, A., Inam, W., Zakharova, L.Y., Zhang, H., and Khutoryanskiy, V.V., 2023. Dynamic light scattering and transmission electron microscopy in drug delivery: A roadmap for correct characterization of nanoparticles and interpretation of results. *Materials Horizons,* 10, pp.5354-5370.

Ghosh, N., Sen, S., Biswas, G., Singh, L.R., Chakdar, D., and Haldar, P.K., 2024. A comparative study of CuO nanoparticle and CuO/PVA-PVP nanocomposite on the basis of dye removal performance and antibacterial activity in wastewater treatment. *International Journal of Environmental Analytical Chemistry*, 104, pp.2234-2254.

González, M.F., Saadatkhah, N., and Patience, G.S., 2024. Experimental methods in chemical engineering: X-ray fluorescence-XRF. *The Canadian Journal of Chemical Engineering*, 102, pp.2004-2018.

Griffin, A., Guo, Y., Hu, Z., Zhang, J., Chen, Y., and Qiang, Z., 2022. Scalable methods for directional assembly of fillers in polymer composites: Creating pathways for improving material properties. *Polymer Composites*, 43, pp.5747-5766.

Hamad, A., Li, L., and Liu, Z., 2016. Comparison of characteristics of selected metallic and metal oxide nanoparticles produced by picosecond laser ablation at 532 and 1064 nm wavelengths. *Applied Physics A*, 122, p.904.

Han, Y., Meng, Z., Wu, Y., Zhang, S., and Wu, S., 2021. Structural colored fabrics with brilliant colors, low angle dependence, and high color fastness based on the mie scattering of Cu_2O spheres. *ACS Applied Materials and Interfaces*, 13, pp.57796-57802.

Holder, C.F., and Schaak, R.E., 2019. Tutorial on Powder X-ray Diffraction for Characterizing Nanoscale Materials. Washington, DC: ACS Publications.

Husham, K.A.F., Khdier, H.M., Saadoon, N.M., and Ahmed, A.M., 2024. Preparation of CuO/PVA nanocomposite thin films for gamma ray attenuation via PLA method. *Journal of Nanostructures*, 14, pp.712-722.

Kambhampati, P., 2021. Nanoparticles, nanocrystals, and quantum dots: What are the implications of size in colloidal nanoscale materials? *The Journal of Physical Chemistry Letters*, 12, pp.4769-4779.

Kanchana, S., Vanitha, N., and Basavaraj, R., 2023a. Structural and optical properties of polyvinyl alcohol/copper oxide (PVA/CuO) nanocomposites. *Solid State Communications,* 370, p.115221.

Kanchana, S., Vanitha, N., Basavaraj, R., and Madivalappa, S., 2023b. Structural and optical properties of polyvinyl alcohol/copper oxide (PVA/CuO) nanocomposites. *Solid State Communications,* 370, p.115221.

Kaur, J., Khanna, A., Kumar, R., and Chandra, R., 2022. Growth and characterization of Cu_2O and CuO thin films. *Journal of Materials Science: Materials in Electronics,* 33, pp.16154-16166.

Kimar, H., and Al-Nesrawy, S.H., 2024. Amelioration and characterization the structural and optical properties of polyvinyl alcohol (PVA)/polyaniline (PANI)/COPPER OXIDE (Cu2O) nanocomposites. *Journal of Nanostructures*, 14, pp.1197-1210.

Kudhur, A.Y., Salim, E.T., Kara, I., Mahdi, R.O., and Ibrahim, R.K., 2024. The effect of laser energy on Cu2O nanoparticles formation by liquid-phase pulsed laser ablation. *Journal of Optics*, 53, pp.1309-1321.

Kumar, R.R., Yu, W.C., Murugesan, T., Chen, P.C., Ranjan, A., Lu, M.Y., and Lin, H.N., 2023. Formation of large-scale MoS2/Cu2O/ZnO heterostructure arrays by in situ photodeposition and application for ppb-level NO2 gas sensing. *Journal of Alloys and Compounds*, 952, p.169984.

Li, Z., Liu, J., Ohki, Y., Chen, G., and Li, S., 2025. Surface flashover in 50 years: II. Material modification, structure optimisation, and characteristics enhancement. *High Voltage*, 10, pp.243-278.

Liu, G.L., and Kazarian, S.G., 2022. Recent advances and applications to cultural heritage using ATR-FTIR spectroscopy and ATR-FTIR spectroscopic imaging. *Analyst,* 147, pp.1777-1797.

Madkhali, O., 2024. A review of novel methods to improve the optical and electrical properties of n-type and p-type sulphides and oxides: Leading the

frontiers of semiconductor technology. *Physica Scripta*, 99, p.022004.

Maier, C., Egger, L., Köck, A., and Reichmann, K., 2025. Investigation of the influence of adhesion layers on the gas sensing performance of CuO/Cu_2O thin films. *Chemosensors*, 13, p.80.

Malik, Z., Khattak, A., Alahmadi, A.A., and Butt, S.U., 2022. Development and investigation of high performance PVA/NiO and PVA/CuO nanocomposites with improved physical, dielectric and mechanical properties. *Materials*, 15, p.5154.

Mallik, M., Monia, S., Gupta, M., Ghosh, A., Toppo, M.P., and Roy, H., 2020. Synthesis and characterization of Cu_2O nanoparticles. *Journal of Alloys and Compounds*, 829, p.154623.

Manjunath, A., Irfan, M., Anushree, K.P., Vinutha, K.M., and Yamunarani, N., 2016. Synthesis and characterization of CuO nanoparticles and CuO doped PVA nanocomposites. *Advances in Materials Physics and Chemistry*, 6, pp.263-273.

Marguí, E., Queralt, I., and De Almeida, E., 2022. X-ray fluorescence spectrometry for environmental analysis: Basic principles, instrumentation, applications and recent trends. *Chemosphere,* 303, p.135006.

Menazea, A., Mostafa, A.M., and Al-Ashkar, E.A., 2020. Effect of nanostructured metal oxides (CdO, Al_2O3, Cu_2O) embedded in PVA via Nd: YAG pulsed laser ablation on their optical and structural properties. *Journal of Molecular Structure*, 1203, p.127374.

Mirzajani, V., Nazarpour-Fard, H., Farhadi, K., and Ghobadian, A., 2022. Copper oxide nano-Catalyst incorporated TEGDN/NC/DAG Propellants: Thermal behaviors and kinetics. *Propellants, Explosives, Pyrotechnics*, 47, p.e202100364.

Mostafa, A.M., Mwafy, E.A., Lotfy, V.F., and Basta, A.H., 2019. Optical, electrical and mechanical studies of paper sheets coated by metals (Cu and Ag) via pulsed laser deposition. *Journal of Molecular Structure,* 1198, p.126927.

Mushtaq, F., Nazeer, M.A., Mansha, A., Zahid, M., Bhatti, H.N., Raza, Z.A., Yaseen, W., Rafique, A., and Irshad, R., 2022. Poly (Vinyl alcohol)(PVA)-based treatment technologies in the remediation of dye-containing textile wastewater. In: *Polymer Technology in Dye-containing Wastewater*. Vol. 2. Springer, Berlin.

Naz, S., Gul, A., Zia, M., and Javed, R., 2023. Synthesis, biomedical applications, and toxicity of CuO nanoparticles. *Applied Microbiology and Biotechnology*, 107, pp.1039-1061.

Oluyemi, F., Ogunmola, E., Ajayi, A., and Olawole, O., 2023. Correlation between molar concentration and properties of sprayed copper oxide thin films. *Results in Optics*, 11, p.100416.

Qian, X.F., Yin, J., Huang, J.C., Yang, Y.F., Guo, X.X., and Zhu, Z.K., 2001. The preparation and characterization of PVA/Ag2S nanocomposite. *Materials Chemistry and Physics*, 68, pp.95-97.

Qiao, T., and Son, D.H., 2021. Synthesis and properties of strongly quantum-confined cesium lead halide perovskite nanocrystals. *Accounts of Chemical Research*, 54, pp.1399-1408.

Ramesh, C., Hariprasad, M., Ragunathan, V., and Jayakumar, N., 2012. A novel route for synthesis and characterization of green Cu2O/PVA nano composites. *European Journal of Applied Engineering and Scientific Research,* 1, pp.201-206.

Rao, J.K., Raizada, A., Ganguly, D., Mankad, M.M., Satayanarayana, S., and Madhu, G., 2015. Investigation of structural and electrical properties of novel CuO-PVA nanocomposite films. *Journal of Materials Science*, 50, pp.7064-7074.

Raship, N., Sahdan, M., Adriyanto, F., Nurfazliana, M., and Bakri, A., 2017. Effect of annealing temperature on the properties of copper oxide films prepared by dip coating technique. *AIP Conference Proceedings,* 2017, p.030121.

Seimela, T.E., 2022. *Synthesis and Characterization of Gold and Silver Nanoparticles for Enhanced Light Collection in Organic Solar Cells.* University of Pretoria, Pretoria.

Singh, R.S., Patidar, R.D., Singh, A.K., Deshmukh, K., Thakur, K., and Gautam, A., 2023. Simple thermal annealing-assisted direct synthesis and optical property study of CuO nanoparticles incorporated polyvinyl alcohol films. *Physica Status Solidi (A)*, 220, p.2300328.

Szczyglewska, P., Feliczak-Guzik, A., and Nowak, I., 2023. Nanotechnology-general aspects: A chemical reduction approach to the synthesis of nanoparticles. *Molecules*, 28, p.4932.

Tkachenko, Y., and Niedzielski, P., 2022. FTIR as a method for qualitative assessment of solid samples in geochemical research: A review. *Molecules*, 27, p.8846.

Vijayashree, K., Rai, K.S., and Demappa, T., 2016. Investigation on nanosized CuO incorporated hydroxypropyl methylcellulose polymer nanocomposite films. *Indian Journal of Advances in Chemical Science S1*, 1, p.5.

Xiao, F., 2012. An efficient layer-by-layer self-assembly of metal-TiO 2 nanoring/nanotube heterostructures, M/T-NRNT (M= Au, Ag, Pt), for versatile catalytic applications. *Chemical Communications*, 48, p.6538-6540.

Xu, L., Zheng, G., Pei, S., and Wang, J., 2018. Investigation of optical bandgap variation and photoluminescence behavior in nanocrystalline CuO thin films. *Optik*, 158, pp.382-390.

Yeap, S.P., Lim, J., Ngang, H.P., Ooi, B.S., and Ahmad, A.L., 2018. Role of particle-particle interaction towards effective interpretation of Z-average and particle size distributions from dynamic light scattering (DLS) analysis. *Journal of Nanoscience and Nanotechnology*, 18, pp.6957-6964.

Zhan, S., Xuefei, D., Zhihao, C., Bao, L., Hao, F., and Jinghu, J., 2024. Precision fabrication of micro-textures array for surface functionalization using picosecond pulse laser. *Optics and Laser Technology*, 177, p.111200.

Zhang, H., Zhu, Q., Zhang, Y., Wang, Y., Zhao, L., and Yu, B., 2007. One-pot synthesis and hierarchical assembly of hollow Cu_2O microspheres with nanocrystals-composed porous multishell and their gas-sensing properties. *Advanced Functional Materials*, 17, pp.2766-2771.

Zhang, J., Zhou, Z., Xiao, B., Zhou, C., Jiang, Z., Liang, Y., Sun, Z., Xiong, J., Chen, G., and Zhu, H. 2023. Visible-light photocatalytic degradation of water-soluble polyvinyl alcohol in aqueous solution by Cu2O@ TiO2: Optimization of conditions, mechanisms and toxicity analysis. *Journal of Environmental Management*, 341, pp.118054.

Zhou, C., Yin, Z., Shao, Y., Zhu, G., Khabibulla, P., Gafurov, A., and Kayumov, J.A., 2025. Research on the construction of Cu_2O photonic crystals on different textile substrates and their mechanical properties. *Textiles*, 5, p.6.